JOURNAL OF Materials CHEMISTRY

A study on the monolayer dispersion of tungsten oxide on anatase

Xiao-Feng Yu, Nian-Zu Wu,* Hui-Zhong Huang, You-Chang Xie and You-Qi Tang

State Key Laboratory for Structural Chemistry of Unstable & Stable Species, Institute of Physical Chemistry, Peking University, Beijing 100871, China.
E-mail: wunz@chem.pku.edu.cn

Received 27th January 2001, Accepted 25th October 2001
First published as an Advance Article on the web 8th November 2001

The monolayer dispersion of tungsten oxide on the surface of anatase has been studied by BET surface area measurements, X-ray diffraction (XRD), X-ray photoelectron spectroscopy (XPS), Fourier transformation infrared spectroscopy (FTIR) and Raman spectroscopy. The results reveal that for the anatase supported tungsten oxide samples, tungsten oxide species can be highly dispersed on the surface of the support and the dispersion state of tungsten oxide species is strongly related to the loading amount of tungsten oxide. In addition, it is found that tungsten oxide can retard the anatase–rutile transformation. When the loading of WO_3 is below its monolayer dispersion capacity, the onset temperature of the anatase–rutile transformation is strongly affected by the dispersed tungsten oxide. Crystalline WO_3 appears when the WO_3 loading is higher than the monolayer dispersion capacity but has little effect on the phase transformation of the samples.

Introduction

The interactions between metal oxides and oxide supports have attracted much attention because of the wide application of supported metal oxide systems. It is well known that supported oxides of transition metals are widely used as catalysts for various reactions. Supported WO_3 catalysts are known for catalyzing different reactions such as WO_3/Al_2O_3 for propene metathesis,[1] WO_3/SiO_2 for olefin disproportionation[2] and WO_3/Fe_2O_3 for the reduction of NO_x in combustion flue gases.[3] Titania supported tungsten oxide catalysts are very efficient for various heterogeneous reactions, such as alkene isomerization and disproportionation.[4–6] Because of the good activity at high temperature, the thermal stability and their low oxidation activity for SO_2, WO_3/TiO_2 catalysts are of interest in industrial applications for the selective catalytic reduction (SCR) of NO by NH_3.[7] Studies carried out by using techniques, *e.g.* XRD, XPS, FT-IR spectroscopy, *etc.*, have shown that the structure of the supported phase and the surface physicochemical properties of the particles are strongly dependent on the method used for their preparation.[8] However, despite the considerable interest in this type of catalyst, most research on supported tungsten catalysts has focused on WO_3/Al_2O_3 and WO_3/SiO_2, while only a few studies concerning the WO_3/TiO_2 system have been reported.[9–21]

In the work reported in this paper a set of samples containing different amounts of tungsten oxide have been prepared using the wet impregnation method. In sample preparations, most authors use ammonium metatungstate or ammonium paratungstate as the precursor of tungsten oxide. In the present paper we dissolved crystalline WO_3 particles in hot ammonium hydroxide solution and then the anatase particles were impregnated in this solution. XRD and XPS results showed that by this means the tungsten oxide species could also be highly dispersed on the surface of the support. It is known that tungsten oxide can stabilize the low temperature anatase phase of TiO_2 and retard the anatase–rutile phase transformation.[10,22] In the present work, it was found that the tungsten oxide could raise the temperature of the anatase–rutile transformation and this effect was strongly related to the loading amount of the tungsten oxide.

Experimental

The TiO_2 support was prepared by hydrolysis of tetrabutyl titanate [$Ti(OBu)_4$], and the product was washed, dried and then calcined at 773 K for 8 h. The required amount of crystalline WO_3 particles were first dissolved in hot aqueous ammonia solution (20 ml; 14.8 mol L^{-1}) and then the titania particles (1 g) were added into this solution (the pH of this solution was maintained at about 11). The impregnation process was performed at 373 K with continuous stirring. Then the samples were dried at 393 K for 2 h and calcined at 773 K for 8 h.

The BET surface areas of the samples were measured using a Micromeritics ASAP 2010 instrument with a computer-controlled measurement system. The samples were evacuated at 623 K to a vacuum below 4 μmHg before measurement.

The identification of crystalline phases was carried out using a BD-86 X-ray diffractometer, employing Cu-Kα (Ni filtered) radiation of wavelength 1.54 Å. The accelerating voltage was 40 kV and the anode current was 20 mA. The data were taken in the range of 10–70° (2θ) with a step size of 0.02° where the time for data collection per step was 0.15 s. The anatase–rutile transformation rate, f, was determined by eqn. (1).[23]

$$f = \frac{1}{1+(0.8\times\frac{I_{A(101)}}{I_{R(110)}})}\times 100\% \quad (1)$$

where $I_{A(101)}$ is the integral intensity corresponding to the (101) peak for anatase and $I_{R(110)}$ is the integral intensity corresponding to the (110) peak for rutile. The XRD line broadening measurements were carried out using a Rigaku Rotaflex diffractometer employing Ni-filtered Cu-Kα radiation (λ = 1.54 Å). The X-ray tube was operated at 40 kV and 120 mA. The DS (divergence slit) was 1°, the SS (scattering slit) was 1.2 mm and the RS (reception slit) was 0.4 mm. The crystal size was obtained using eqn. (2):

$$D = K\lambda/(B-B_0)\cos\theta \quad (2)$$

where D is the crystal size, θ is the diffraction angle, K is a constant (0.9), B_0 is the FWHM of diffraction peak when the crystallites are very large and show no line broadening beyond instrumental effects, and B is the FWHM of the sample.

DOI: 10.1039/b100971k

This journal is © The Royal Society of Chemistry 2001

XPS spectra were obtained using a VG-ESCALAB 5 spectrometer. An Al-K$\alpha_{1,2}$ X-ray source was used and the anode was operated at 9 kV and 18.5 mA. The chamber pressure was kept at 10^{-8} Torr. The pass energy of analyzer was fixed at 50 eV. The XPS peak intensity ratio of the energy levels for W 4d and Ti 2p was taken as a measurement of the surface concentration of tungsten oxide on TiO_2.

Raman spectra were recorded on a Nicolet 950 Fourier transform spectrometer with a Ge detector cooled by liquid nitrogen. Raman excitation at 1064 nm was provided by a Nd : YVO_4 laser. The laser power measured at the powder sample was 400 mW, and spectra were accumulated for 1000 scans at 8 cm^{-1} resolution in backscattering geometry.

FT-IR spectra were taken with a Nicolet 750 Fourier transform infrared spectrometer operated with a spectral resolution of 4 cm^{-1}. Samples were pressed into wafers after the mixture and ground with KBr.

Results and discussion

The specific surface areas of the WO_3/TiO_2 samples calcined at 773 K, measured using the BET method are listed in Table 1. From Table 1 it can be seen that the surface areas decrease with an increase of tungsten oxide loading. This change is very small when the WO_3 loading amount is small but the decrease becomes more obvious when the WO_3 loading is very high.

XRD peak FWHM values were measured and crystal sizes of the samples calculated using eqn. (2) (and listed in Table 2). After the WO_3 was loaded on anatase, the crystal sizes of the samples calcined at 773 K were not obviously changed. It seems that after the impregnation and calcination at 773 K, the loading of tungsten oxide has no appreciable effect on the crystal size of the TiO_2 support.

The XRD patterns (2θ in the range 20–29°) of selected WO_3/TiO_2 samples with various WO_3 loadings are shown in Fig. 1. The patterns are almost coincident with that of anatase and no peaks corresponding to the crystalline phase of WO_3 can be observed in samples with low WO_3 loading (profiles a and b of Fig. 1). However, for samples with high WO_3 loading, such as samples d and e, the characteristic peaks of crystalline WO_3 can be clearly seen. The results suggest that the tungsten oxide exists as highly dispersed species on the support at low loadings and crystalline WO_3 appears in samples of high loadings.

For the supported metal oxide samples, it has been shown that XPS metal-to-support intensity ratios can provide important information regarding the dispersion and crystalline size of the supported metal particles.[24,25] Because the strongest XPS peak of WO_3, *i.e.*, W 4f, is overlapped by the Ti 3p peak and can not be measured precisely, the W 4d peak is instead used to quantify the amount of tungsten on the support. The correlation between the W 4d/Ti 2p XPS intensity ratios and the loading amount of WO_3 in the WO_3/TiO_2 samples is shown in Fig. 2. Two lines with different slopes can be discerned. The intersection point of the two lines is at about 69 mg WO_3 (g TiO_2)$^{-1}$. For WO_3 loading below this value, the slope of $I_{W\ 4d}/I_{Ti\ 2p}$ *vs.* the WO_3 loading is steep whilst above this value it is much less so. The different slopes of the two straight lines can be explained if there are different states in the tungsten oxide species supported on anatase. When the WO_3 loading is below 69 mg WO_3 (g TiO_2)$^{-1}$ tungsten oxide exists as highly dispersed species on the surface of the support TiO_2, so that $I_{W\ 4d}/I_{Ti\ 2p}$ increases rapidly with the increase of WO_3 loading. However, when the WO_3 loading is beyond 69 mg WO_3 (g TiO_2)$^{-1}$, crystalline WO_3 starts to form. Since for a given amount of WO_3, the contribution of crystalline WO_3 to $I_{W\ 4d}$ is much smaller than that of highly dispersed WO_3, the degree of increase of $I_{W\ 4d}/I_{Ti\ 2p}$ is much smaller once crystalline WO_3 is deposited. The point of intersection of the two lines can be regarded as a threshold corresponding to the monolayer dispersion capacity. The monolayer dispersion capacity of the WO_3/TiO_2 system calcined at 773 K is about 69 mg WO_3 (g TiO_2)$^{-1}$. On the basis of the BET surface area of anatase (43.8 $m^2\ g^{-1}$), the monolayer dispersion capacity can also be expressed as 4.1 W^{6+} ($nm^2\ TiO_2$)$^{-1}$. The above results are consistent with the conclusion obtained from XRD studies that only highly dispersed tungsten oxide species exist in the low loading samples whilst an additional crystalline WO_3 phase is formed in samples with WO_3 loadings higher than the monolayer dispersion capacity. Furthermore, it can be concluded from XRD and XPS results that crystalline WO_3 can also be dispersed as a monolayer on the TiO_2 support by impregnation.

Raman spectra of the WO_3/TiO_2 samples were obtained. The anatase support shows bands at 152, 403, 518 and 642 cm^{-1}.

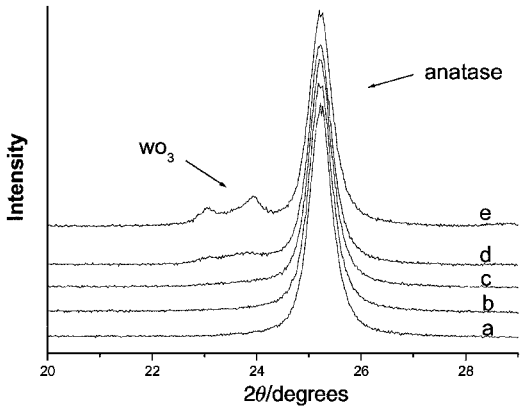

Fig. 1 X-Ray diffraction diagrams for samples: (a) 19.7 mg WO_3 (g TiO_2)$^{-1}$, (b) 40.1 mg WO_3 (g TiO_2)$^{-1}$, (c) 69.7 mg WO_3 (g TiO_2)$^{-1}$, (d) 100.6 mg WO_3 (g TiO_2)$^{-1}$ and (e) 171.3 mg WO_3 (g TiO_2)$^{-1}$. The 2θ range is 20–29°.

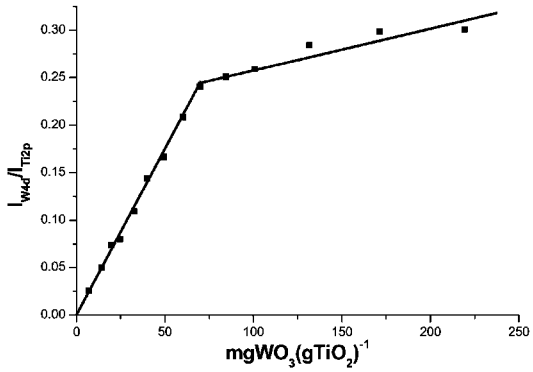

Fig. 2 XPS peak intensity ratio $I_{W\ 4d}/I_{Ti\ 2p}$ *vs.* the content of WO_3 in WO_3/TiO_2 samples.

Table 1 BET surface areas of some samples

Sample/mg WO_3 (g TiO_2)$^{-1}$	Pure anatase	6.9	24.6	49.3	69.7	131.6	219.4
BET surface area/$m^2\ g^{-1}$	43.8	43.4	42.9	43.1	42.5	37.9	35.4

Table 2 The FWHM and crystal size of some samples

Sample/mg WO_3 (g TiO_2)$^{-1}$	Pure anatase	14.1	40.1	69.7	100.6	171.3
$B-B_0$ (FWHM)/°	0.335	0.324	0.33	0.332	0.329	0.328
crystal size, D/Å	256	265	260	258	261	262

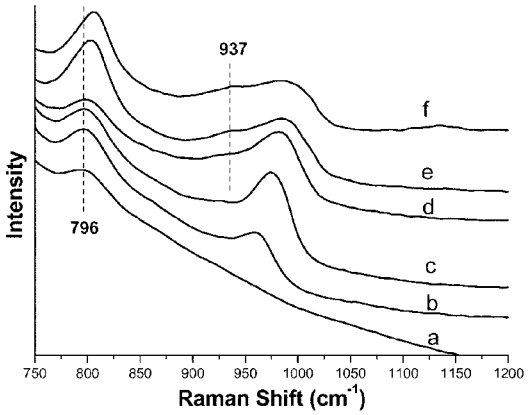

Fig. 3 Raman spectra in the region 750–1200 cm^{-1} of samples: (a) anatase, (b) a sample with WO_3 coverage of 19.7 mg WO_3 (g TiO_2)$^{-1}$ or 0.28 monolayer, (c) 40.1 mg WO_3 (g TiO_2)$^{-1}$ or 0.58 monolayer, (d) 69.7 mg WO_3 (g TiO_2)$^{-1}$ or 1.00 monolayer, (e) 100.6 mg WO_3 (g TiO_2)$^{-1}$ or 1.46 monolayer and (f) 171.3 mg WO_3 (g TiO_2)$^{-1}$ or 2.48 monolayer.

Fig. 3 shows Raman spectra in the range 750–1200 cm^{-1} for different WO_3 loadings. The peak positions of the Raman spectra are shown in Table 3.

It can be seen that all the WO_3/TiO_2 samples show a band at about 796 cm^{-1} and the wavenumber of this band shifts to higher position (from 796 to 808 cm^{-1}) with the increase of WO_3 loading. The Raman spectrum of anatase also shows a band at 796 cm^{-1} which is the first overtone of the 403 cm^{-1} anatase band.[26] Thus the bands for the samples at 796 cm^{-1} do not belong to tungsten oxide but to anatase. It is noteworthy that the wavenumber and the intensity of this band remains almost unchanged in samples b–d with WO_3 loadings lower than or close to the monolayer dispersion capacity. When the loading of WO_3 exceeds the monolayer dispersion capacity (samples e and f), the Raman band at 808 cm^{-1} appears and the intensity of this band increases remarkably. This band can be attributed to the W–O stretching mode of crystalline WO_3, which has three characteristic peaks around 808, 719 and 276 cm^{-1}.[27] It can be concluded that when the WO_3 loading is beyond its monolayer dispersion capacity crystalline WO_3 begins to appear.[28] This result confirms the XRD and XPS conclusions indicating that the tungsten oxide monolayer is achieved for tungsten loading just below 69 mg WO_3 (g TiO_2)$^{-1}$ and crystalline WO_3 appears in samples with higher loading.

At low WO_3 loading another tungsten oxide species is observed which exhibits a broad and intense band at 958 cm^{-1} (sample b in Fig. 3). With the increase of the WO_3 loading this band shifts to higher wavenumber (from 958 to 986 cm^{-1}). This band can be attributed to the symmetric W=O stretching mode of surface dispersed bidimensional tungsten oxide species.[9,12,29] Similar observations have been made for tungsten oxide on alumina[30] and on titania[12,17] where the Raman peaks shift to higher wavenumbers with the increase of WO_3 loading. In the WO_3/Al_2O_3 system,[30–32] it has been reported that at low WO_3 loading, tetrahedrally coordinated tungsten oxide (WO_4) is the main species on the surface of the support whilst at higher loading the octahedrally coordinated tungsten oxide species (WO_6) is present and becomes predominant. Similarly to the WO_3/Al_2O_3[30–32] and WO_3/TiO_2 systems,[18] it can be concluded that the band at 958 cm^{-1} belongs to the symmetric stretch of the W=O bond within distorted WO_4 species and at moderate WO_3 loading the band at 973–986 cm^{-1} should be mostly due to the W=O bond in distorted WO_6 species.

With the band of W=O shifting to higher wavenumber, another tungsten oxide species appears. Even at very low coverage, such as b and c in Fig. 3, there is a very weak and broad peak at the shoulder of the W=O peak at about 910–950 cm^{-1}. When the loading of WO_3 is near or beyond the monolayer dispersion capacity, this peak becomes more obvious. Tungsten oxide reference compounds which possess bridging W–O–W groups, such as $Na_2W_2O_7$, $K_2[W_2O_3(O_2)_4(H_2O)_2]$ or $(NH_4)_6H_2$- $W_{12}O_{40}$, reveal bands in the 900–1000 cm^{-1} region (symmetric stretch), 800–900 cm^{-1} region (asymmetric stretch), 500–650 cm^{-1} region (W–O–W symmetric stretch), 300 cm^{-1} region (bending) and 150–250 cm^{-1} region (W–O–W bending).[31] Because the bands of anatase at 518 and 642 cm^{-1} are very strong, no other peak is found in the 500–650 cm^{-1} region. However, in the 150–250 cm^{-1} region, another band is found, as shown in Fig. 4. The band at 198 cm^{-1} is one of the bands of anatase. With the increase of the WO_3 loading, especially beyond the monolayer dispersion capacity, a band at 202 cm^{-1} becomes pronounced. In view of the fact that the change is not striking, another series of WO_3/TiO_2 samples were prepared again by the same process and their Raman spectra show the same trend as in Fig. 4. It is suspected that the band at 202 cm^{-1} is diagnostic of W–O–W linkages. The appearance of the bands at about 930–941 cm^{-1} (in Fig. 3) and 202 cm^{-1} (Fig. 4) indicates the presence of polytungstate species composed of WO_4 and WO_6 units joined in chains on the anatase surface at higher surface coverage as found in the WO_3/Al_2O_3 system.[31] Vuurman and Wachs reported that alumina-supported molybdenum oxide, tungsten oxide, vanadium oxide and niobium oxide systems also reveal the presence of M–O–M linkages (the Raman bands of W–O–W are at ~590 and ~215 cm^{-1}) which are indicative of polymeric structure at higher surface coverage.[33] Horsley *et al.* found that the Raman spectra of WO_3/Al_2O_3 samples indicate W–O–W bonds at 250 cm^{-1} at low coverage.[31] A similar result obtained by Hilbrig *et al.* using EXAFS shows that for the WO_3/TiO_2 system the W–O–W structure exists at both low and high WO_3 coverage.[16] From these results, it can be concluded that the tungsten oxide species are highly dispersed as isolated tetrahedra (WO_4) at low coverage; at higher WO_3 loading octahedrally coordinated tungsten oxide species (WO_6) appear and the ratio of WO_6 to WO_4 increases with the increase of

Table 3 The Raman shift of some samples. Letters a–f refer to the curves in Fig. 3

Sample	Raman shift/cm^{-1}		
a	796		
b	796		958
c	796	930	973
d	798	937	981
e	804	937	986
f	808	941	986

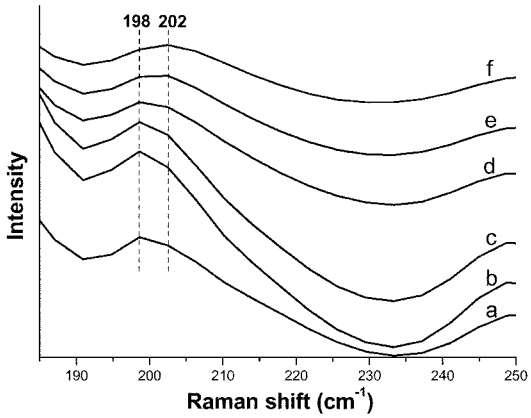

Fig. 4 Raman spectra in the region 185–250 cm^{-1} of samples a–f (the same as those in Fig. 3).

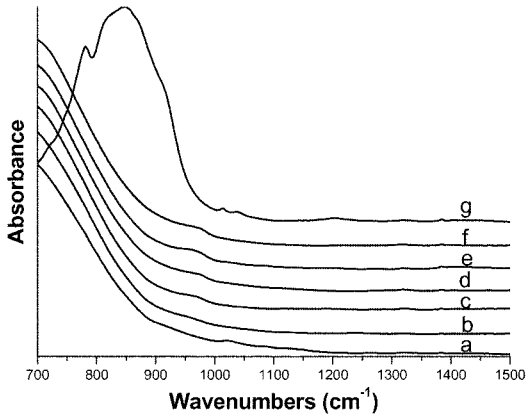

Fig. 5 FT-IR spectra in the region 700–1500 cm^{-1} of samples a–f (the same as those in Fig. 3) whilst g is the spectrum of crystalline WO_3.

WO_3 loading. At the same time the tetrahedrally and octahedrally coordinated tungsten oxide species begin to come into contact with each other and form cross linked structures (polytungstate species).[18]

From all the results obtained from Raman spectra, the following conclusions can be drawn. At low WO_3 loading the tungsten oxide is dispersed as isolated tetrahedrally coordinated structures on the surface of anatase. With increasing tungsten oxide loading, tetrahedrally and octahedrally coordinated structures, as well as polytungstates are found,[18] while with more than one monolayer coverage on the anatase support, crystalline WO_3 is formed.

FT-IR spectra of WO_3/TiO_2 samples with different WO_3 loadings are shown in Fig. 5. The IR spectrum of TiO_2 (Fig. 5(a)) shows the absorption of the anatase form with a broad and strong band in the 400–900 cm^{-1} region. For WO_3/TiO_2 samples, the peak at 950–990 cm^{-1} is distinct, as shown in spectra (b)–(f). With an increase of the WO_3 loading, this peak becomes more and more distinct. These peaks, due to tungsten oxide species, do not correspond to that of crystalline WO_3 (Fig. 5(g)) and should correspond to the stretching mode of the W=O bond in dispersed tungsten oxide species.[19] Also, many other researchers have reported that the Raman and IR bands due to terminal W=O bonds, at the corresponding tungsten oxide loadings, are observed at similar wavenumbers.[12,33,34] This result is in agreement with the conclusions drawn from the Raman spectra mentioned above. Because the band of anatase at 400–900 cm^{-1} is so broad and strong, it is difficult to obtain further information from the IR spectra.

Monolayer dispersion is a common or even ubiquitous event

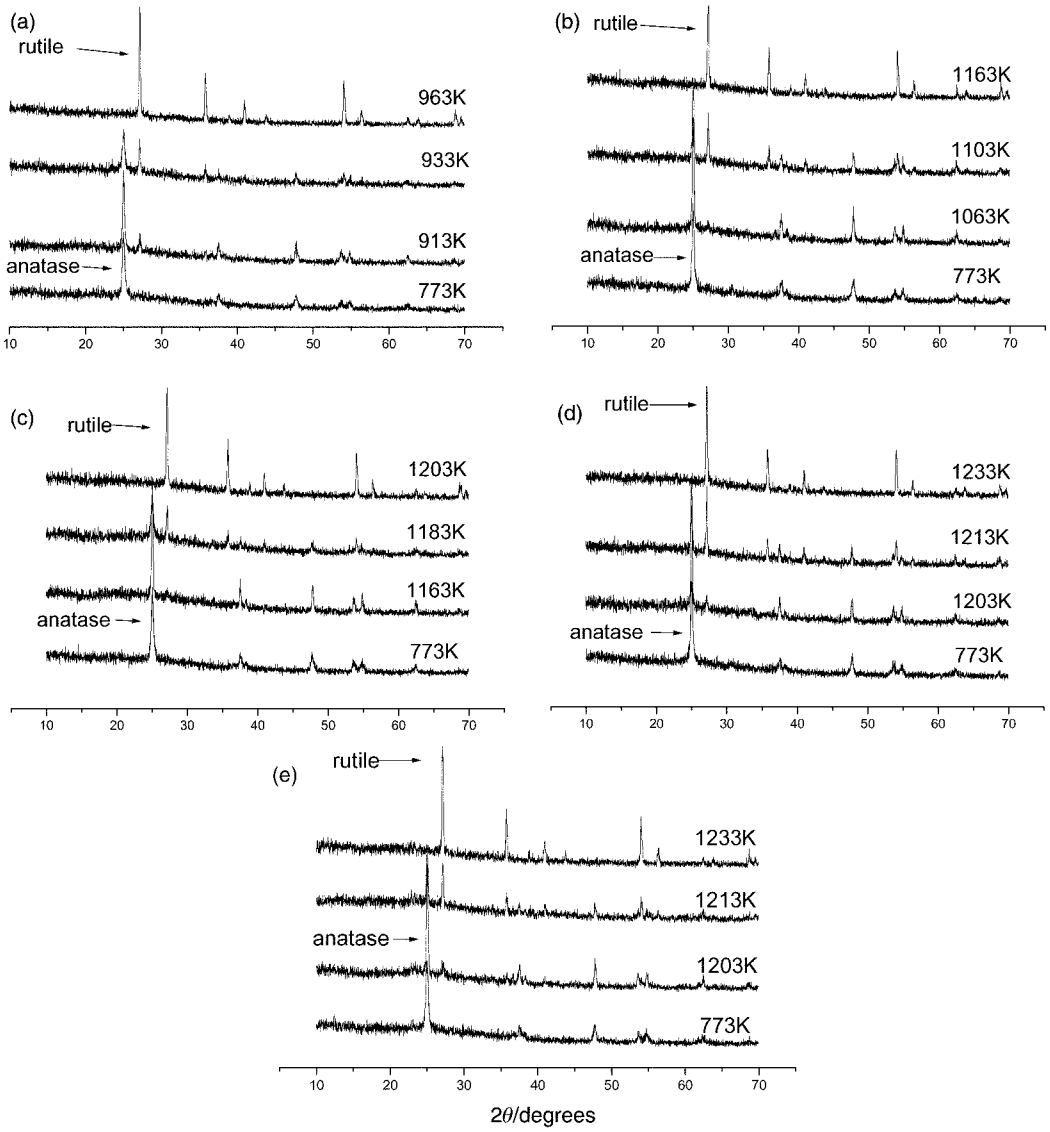

Fig. 6 XRD profiles, as a function of temperature, of (a) pure anatase; (b) a sample with WO_3 coverage 14.1 mg WO_3 (g TiO_2)$^{-1}$ or 0.20 monolayer; (c) 40.1 mg WO_3 (g TiO_2)$^{-1}$ or 0.58 monolayer; (d) 69.7 mg WO_3 (g TiO_2)$^{-1}$ or 1.00 monolayer and (e) 100.6 mg WO_3 (g TiO_2)$^{-1}$or 1.46 monolayer, after calcination for 4 h.

Table 4 The onset phase transformation temperature (T_{onset}) and the temperature at which anatase is completely transformed to rutile (T_{final}) of samples after calcination for 4 h. Data for samples on which the loadings of WO_3 are larger than 69.7 mg WO_3 (g TiO_2)$^{-1}$ are almost the same as the sample of 69.7 mg WO_3 (g TiO_2)$^{-1}$

Loading of WO_3/ mg WO_3 (g TiO_2)$^{-1}$	Coverage of WO_3/ monolayers	T_{onset}/K	T_{final}/K
pure anatase	0	913	963
3.5	0.05	1003	1073
14.1	0.20	1063	1163
24.6	0.36	1123	1193
40.1	0.58	1163	1203
69.7	1.0	1203	1233
100.6	1.45	1203	1233
219.4	3.18	1203	1233

rather than a rare occurrence. Furthermore, there are many unique effects when compounds disperse as monolayers on supports.[35] In our previous paper,[36] we found that dispersed copper oxide on an anatase support could lower the anatase–rutile phase transformation temperature and this influence was strongly related to the loading of copper oxide. By contrast, tungsten oxide retards the anatase–rutile phase transformation.[10,22] To study the influence of dispersed tungsten oxide on the anatase–rutile transformation, powder X-ray diffraction was used to determine the phase of titania present at different temperatures. Fig. 6(a)–(e) show XRD spectra indicating the influence of tungsten oxide at different contents on the anatase–rutile phase transformation after calcination for 4 h. We defined the temperature at which 1% of the anatase has transformed to rutile after calcination for 4 h employing the transformation rate equation (eqn. (1)) as the onset phase transformation temperature (T_{onset}). It is found that the tungsten oxide can noticeably retard the transformation and raise the transformation temperature. Fig. 6(a) shows the results of heating a pure anatase sample. It is found that at 773 K the titania phase is anatase but that after calcination at 913 K for 4 h, diffraction peaks of rutile were observed, and that anatase was completely converted to rutile after calcination at 963 K for 4 h. This behavior was altered when a WO_3 monolayer was dispersed on anatase. Fig. 6(b) shows the results of heating a 14.1 mg WO_3 (g TiO_2)$^{-1}$ sample. The anatase phase was maintained up to about 1053 K and the initiation transformation temperature (1063 K) is about 150 K higher than that of the pure anatase sample. After further calcination at 1163 K the anatase was completely transformed to rutile. The other samples showed similar effects. Data of the onset phase transformation temperature and the temperature at which anatase is completely transformed to rutile for samples are given in Table 4.

Furthermore, the effect of enhancing the onset transformation temperature is strongly related to the loading amount of tungsten oxide. Fig. 7 shows the onset transformation temperature as a function of the WO_3 loading. When the WO_3 loading is low, the onset transformation temperature is enhanced dramatically while when the WO_3 loading is near the monolayer dispersion capacity, 69.7 mg WO_3 (g TiO_2)$^{-1}$, the rising trend is slowed. When the WO_3 content is beyond the monolayer dispersion capacity, there is no obvious further change and the temperature is maintained at about 1203 K up to 219.4 mg WO_3 (g TiO_2)$^{-1}$.

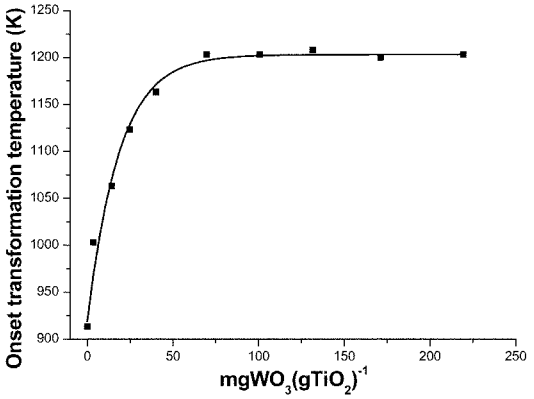

Fig. 7 Onset transformation temperature *vs.* WO_3 loading.

All these results lead to the conclusion that after WO_3 is loaded on the anatase support, the anatase–rutile phase transformation was raised and was related to the extent of WO_3 loading. In all these measurements, no other crystalline phases were detected by XRD (besides WO_3, anatase and rutile) in the samples even upon calcination at 1233 K for 4 h. These results lead to the conclusion that the WO_3 and the anatase support have not reacted to form any new compounds and that the presence of the monolayer dispersed tungsten oxide simply influences the anatase–rutile transformation. In our previous report, it was found that the monolayer dispersed copper oxide could accelerate the anatase–rutile phase transformation.[36] It has also been confirmed that[37] the conversion of zirconia from the tetragonal to the monoclinic form at high temperature starts at the surface of the particles and proceeds towards the center of the crystal. It is very likely that in the present experiment the same process occurs in the anatase–rutile transformation. The highly dispersed tungsten oxide forms strong surface bonds with the anatase particles as shown by Raman and FT-IR results, which will affect the anatase–rutile transformation. The surface induced anatase–rutile transformation of tungsten oxide-loaded anatase is much more difficult than that of pure anatase. From Fig. 7, it is seen for a sample with low WO_3 loading, that the onset transformation temperature was enhanced dramatically, and the higher the WO_3 loading, the stronger the retarding effect. When the WO_3 loading exceeded the monolayer dispersion capacity, the available surface of anatase was occupied by dispersed tungsten oxide, and crystalline WO_3 appears. Because the crystalline WO_3 does not come into contact with the surface of the support, the phase transformation will no longer be affected and the phase transformation temperature should remain unchanged.

Conclusion

XRD and XPS show that tungsten oxide can be highly dispersed as a monolayer on anatase by impregnation using crystalline WO_3. The dispersion capacity of WO_3 on anatase is about 69 mg WO_3 (g TiO_2)$^{-1}$ or 4.1 W^{6+} (nm^2 TiO_2)$^{-1}$ by XPS. Raman and FT-IR spectra show that different tungsten oxide species appear successively with increase of WO_3 loading. Furthermore, the highly dispersed tungsten oxide can retard the anatase–rutile transformation markedly and is strongly related to the WO_3 loading. When the loading of WO_3 is beyond the dispersion capacity, crystalline WO_3 appears, which has little effect on the phase transformation of the support as compared to the highly dispersed tungsten oxide.

Acknowledgements

This work was supported by project No. 29733080 from the National Natural Science Foundation of China and the Major State Basic Research Development Program (Grant No. G2000077503) from the Science and Technology Ministry of China.

References

1 R. Thomas and J. A. Moulijn, *J. Mol. Catal.*, 1982, **15**, 157.
2 G. C. Bailey, *Catal. Rev.*, 1969, **3**, 37.

3 M. Imanari, Y. Watanabe, S. Matsuda and F. Nakajima, in *Proceedings of the 7th International Congress on Catalysis, Tokyo, 1980*, Elsevier, Amsterdam, 1981, p 41.
4 M. Ai, *J. Catal.*, 1977, **49**, 305.
5 T. Yamaguchi, Y. Tanaka and K. Tanabe, *J. Catal.*, 1980, **65**, 442.
6 T. Yamaguchi, S. Nakamura and H. Naguno, in *Proceedings of the 8th International Congress on Catalysis*, Verlag Chemie, Weinheim, Germany, 1984, vol. 5, p. 579.
7 S. Morikawa, K. Takahashi, J. Mogi and S. Kurita, *Bull. Chem. Soc. Jpn.*, 1982, **55**, 2254.
8 G. A. Somorjai, in *Introduction to Surface Chemistry and Catalysis*, Wiley, New York, 1994.
9 S. S. Chan, I. E. Wachs, L. L. Mrrell, L. Wang and W. K. Hall, *J. Phys. Chem.*, 1984, **88**, 5831.
10 S. H. Han, H. S. Kim and K. Kim, *Bull. Korean. Chem. Soc.*, 1991, **12**, 80.
11 G. C. Bond, S. Flamerz and L. Van Wijk, *Catal. Today*, 1987, **1**, 229.
12 M. A. Vuurman, I. E. Wachs and A. M. Hirt, *J. Phys. Chem.*, 1991, **95**, 9928.
13 K. S. P. Rao, G. Muralidhar, S. Khajamasthan and V. S. Subrahmanyam, *React. Kinet. Catal. Lett.*, 1988, **37**, 181.
14 M. Valigi, S. DeRossi, D. Gazolli and G. Minelli, *J. Mater. Sci.*, 1985, **20**, 71.
15 D. C. Vermaire and P. C. Van Berge, *J. Catal.*, 1989, **116**, 309.
16 F. Hilbrig, H. E. Gobel, H. Knozinger, H. Schmelz and B. Lengerler, *J. Phys. Chem.*, 1991, **95**, 6973.
17 R. B. Quincy, M. Houalla and D. Hercules, *Fresenius' J. Anal. Chem.*, 1993, **346**, 676.
18 A. Scholz, B. Schnyder and A. Wokaun, *J. Mol. Catal. A*, 1999, **138**, 249.
19 G. Ramis, G. Busca, C. Cristiani, L. Lietti, P. Forzatti and F. Bregani, *Langmuir*, 1992, **8**, 1744.
20 J. Engweiler, J. Harf and A. Baiker, *J. Catal.*, 1996, **159**, 259.
21 C. Martin, G. Solana, V. Rivers, G. Marci, L. Palmisano and A. Sclafani, *Catal. Lett.*, 1997, **49**, 235.
22 K. Kenevey, M. A. Morris, J. Cunningham and G. Ferrand, *Key Eng. Mater.*, 1996, **118–119**, 303.
23 R. A. Spurr and H. Mysers, *Anal. Chem.*, 1957, **29**, 760.
24 F. P. Kerkhof and J. M. Moulijn, *J. Phys. Chem.*, 1979, **83**, 1612.
25 S. C. Fung, *J. Catal.*, 1979, **58**, 454.
26 U. Balachandran and N. G. Eror, *J. Solid State Chem.*, 1982, **42**, 276.
27 N. C. Raman, D. L. Sullivan, J. G. Ekerdt, J. M. Jehng and I. E. Wachs, *J. Catal.*, 1998, **176**, 143.
28 S. S. Chan, I. E. Wachs and L. L. Mrrell, *J. Catal.*, 1984, **90**, 150.
29 G. Deo and I. E. Wachs, *J. Phys. Chem.*, 1991, **95**, 5889.
30 M. M. Ostromecki, L. J. Burcham, I. E. Wachs, N. Ramani and J. G. Ekerdt, *J. Mol. Catal. A*, 1998, **132**, 43.
31 J. A. Horsley, I. E. Wachs, J. M. Brown, G. H. Via and F. D. Hardcastle, *J. Phys. Chem.*, 1987, **91**, 4014.
32 J. M. Stencel, *Raman Spectroscopy for Catalysis*, van Nostrand Reinhold, New York, 1990.
33 M. A. Vuurman and I. E. Wachs, *J. Phys. Chem.*, 1992, **96**, 5008.
34 D. S. King, M. Ostromecki and I. E. Wachs, *J. Mol. Catal. A*, 1996, **106**, 93.
35 Y. C. Xie and Y. Q. Tang, *Adv. Catal.*, 1990, **37**, 1.
36 X. F. Yu, N. Z. Wu, Y. C. Xie and Y. Q. Tang, *J. Mater. Chem.*, 2000, **10**, 1629.
37 J. R. Anderson, *Structure of Metallic Catalysts*, Academic Press, London, 1975, p. 62.